SAND2022-2972C

ARMA 22-726

Fracture Detection of Lab Scale Energetic Stimulation

Robey, R.E. and Pope, J.S.
Sandia National Laboratories, Albuquerque, New Mexico, United States
Vorobiev, O.Y.
Lawrence Livermore National Laboratory, Livermore, California, United States
Torres S.M, Hargather, M.J., Kimberley, J., and Mann, D.
New Mexico Institute of Mining and Technology, Socorro, New Mexico, United States

This paper was prepared for presentation at the 56th US Rock Mechanics/Geomechanics Symposium held in Santa Fe, New Mexico, USA, 26-29 June 2022. This paper was selected for presentation at the symposium by an ARMA Technical Program Committee based on a technical and critical review of the paper by a minimum of two technical reviewers. The material, as presented, does not necessarily reflect any position of ARMA, its officers, or members. Electronic reproduction, distribution, or storage of any part of this paper for commercial purposes without the written consent of ARMA is prohibited. Permission to reproduce in print is restricted to an abstract of not more than 200 words; illustrations may not be copied. The abstract must contain conspicuous acknowledgement of where and by whom the paper was presented.

ABSTRACT: Stimulation of lab scale boreholes was studied using small explosives for improving the development of fracture networks in engineered rock surrogates. The experimental series examines the confluence of initial stress states, orientation of induced discontinuities and their interaction with source generated fracture growth. Density and stress response to the energetic was measured using high-speed schlieren imaging through the transparent polymethyl methacrylate (PMMA) sample. Outer surfaces were instrumented with an acoustic emissions (AE) array to detect 3D location of fracture evolution between wellbores. Prior to testing, the experiments were simulated to predict the generation of a shock induced fracture network between single and multiple wellbores in a variety of stress states. The quantification of wave arrivals, fracture growth, and development of the fracture network in transparent PMMA material is used as further validation against computational models. Understanding the conditions under which fractures propagate in the multivariate environment with small energetics results in improved modeling capability of larger scale wellbores and sources. The present work is part of a broader effort to accurize computational models necessary to predict formation interconnectivity established with energetics in low permeability reservoirs typical of enhanced geothermal systems (EGS).

1. INTRODUCTION

Acoustic emission (AE) sensing has become a pertinent technology to the observe flaws in a variety of media. Investigators can use arrays of omni-directional probes to observe energy radiating in the form of compression waves released from fracture tips, voids or features as they are distorted under load. Patterns in radiated energy may be correlated to spatial-temporal formation of microfractures. This method has been applied to the field of geomechanics where fractures grow due to an induced stress state, or when energy is radiated from an existing feature such as slip plane. In this study, stress was induced for the purposes of studying lab scale stimulation of geothermal wellbores using energetic sources so that computational models could be further informed by the acoustic emissions of fractures driven by energetics.

The stimulation of geothermal wells with energetics is being evaluated such that environmental impacts and well costs may be reduced [1]. Subsurface explosive sources release energy rapidly, generating strong compressive waves in situ exceeding dynamic properties of neighboring geologic materials and overburden stresses. Stimulation evaluation of hard rock present in geothermal reservoir has been previously performed by Grubelich [2] and others which was primarily focused on shallow field level studies. In one campaign, post stimulation cross hole sonic logs showed some decrease in wave velocity of a rhyolite formation, suggesting a change in permeability caused by new fracture placement from the energetic source. Grubelich's work was not performed in a producing geothermal asset, so change in production could not be observed. The experiment was a fair analog of an enhanced geothermal system (EGS) where at least one injection well and one production well should share a common fracture network for heat transfer to the working fluid in an igneous reservoir. In contrast, experiments performed by Mumma et.al. [3] showed no improvement of well productivity in a steam producing asset. Rather

than improving steam drainage by increasing reservoir contact, an undesirable change of local production resulted from rock face sloughing and subsequent wellbore bridging. A possible explanation of why this could occur was proposed by Cuderman [4] where it was demonstrated that the rise-time of pressure in a wellbore caused differences in the way source gasses perform work. Extremes of these observations can be described in by fast rise in gas production times creating crushing damage versus a slow rise source causing fractures distal from the rock face. While Cuderman' s observations were in ash fall tuff, the phenomenon of fracture generation versus crushing is likely multi-variate with dependencies on source, energy transmission and reservoir geology. The present study is designed to observe source induced fracture growth in simulated lab scaled geothermal reservoirs.

A previous campaign in this study [5] validated particle velocities exceeding 15 m/s and shock velocities over 2.5 km/s in PMMA cubes using 750 mg of PETN. Post-test examination of the cubes revealed expected crushing in the near wellbore volume, and discrete fractures that had formed due to remnant cavity pressure. This provided greater reservoir contact than the borehole formed into the simulated PMMA reservoir. Further study of the high-speed imaging of the transparent material revealed weak elastic waves emanating from fracture tips within time regimes similar to the prompt waves and their reflections.

While exciting, the shadowgraph technique had limitations in observing fracture growth within the transparent cubes. Optical clarity is affected by the presence of fractures, and while this does not influence observation of prompt shock, later time artifacts may be obscured by the change in refractive index. It was noted that gas driven fractures growing perpendicular to the field of view (FOV) created opaque features due to gas filled apertures. The lack of transparency obscured the presence of other fractures not progressing substantially in the direction perpendicular to the FOV. Further, shadowgraph imaging would not be applicable for opaque geologic materials when the study pivoted to rock targets.

Photon doppler velocimetry (PDV) was highly capable of measuring prompt shock velocities at the PMMA free surfaces, however the weak elastic waves from fracture growth were not readily observed and were highly obscured within larger wavelets making correlation to discrete fractures difficult.

While work presented herein does intend to fully explain the interrelation of source characteristics and target damage, the spatial-temporal assessment of crushing and fracture at a lab scale is critical for quantification of damage evolution. Even more so when opaque materials are stimulated with sources designed to induce changes in rise-time and subsequent differences in damage characteristics.

In this phase of the study several research thrusts were explored. First the introduction of artifacts into the PMMA targets to replicate the reality of subsurface rock contact and geologic layers intersecting drilled well trajectories. This would allow for instrumented observation of fracture growth around known discontinuities. Secondly, uniaxial stress (σ_1) was added to the cubes to represent the earths overburden stresses so fracture directionality could be assessed. Lastly AE instrumentation was added to capture the fracture release waves to co-witness damage observed with highspeed imaging so that spatial-temporal location could be trusted in an opaque material. Ultimately these thrusts are designed to understand physics of the phenomena and to inform the computational model which is necessary for field level simulation studies.

EXPERIMENTAL APPROACH

1.1. Source & Target Selection

Challenges exist for selecting sources for lab scale tests. This is based on the size limitation of explosives and the boundary loss effects of detonation energies in small diameter boreholes. Commercially available explosives such as HMX, RDX and PETN were evaluated for gas production using CHEETAH [6] thermochemical calculation code in previous experiments. Experience with PETN revealed potential failure points of placing bulk powder into the slim borehole with a slim aspect ratio (L/D = 20). To mitigate potential inconsistencies of initiation and energy transmission to the PMMA cube, investigators moved to a Teledyne RISI RP-80 with a plastic shell. The off the shelf source was expected to lower energy input into the borehole due to the smaller mass of explosives; 4.5 kJ vs 1.1kJ. However, the difference of explosive type would change shock transmission conditions due to the increased CJ pressure for RDX at the output pressing of the detonator [7]. In these tests multiple detonators were wired in parallel to prevent function time variation from affecting reliability [8]. By utilizing two detonators, overall energy input to the cube was reduced by 50% compared to the previously utilized single 750 mg PETN source.

The PMMA cubes were prepared in several configurations. First as a as single piece mono block which were constructed from 30 cm thick cast sheets and cut to size. These were expected to be most advantageous for measuring waves and fractures with minimal introduction of defects or artifacts. Layering was introduced by stacking 5 cm thick PMMA sheets and bonding with acrylic cement (methylene chloride, trichlorethylene and methyl methacrylate monomer). The bonds were cured while a stress normal to the joint was applied to minimize poor flatness characteristics of the thinner 5 cm sheets. After curing, the cubes were machined for squareness, mechanically polished, and before flame polishing on the surfaces on interest. This

Commented [RRE1]: Joe is this correct?

method created thin joints with optical clarity, which depending on viewing angle, approached that of the native material. These joints were mechanically competent, and bonding was tested to stress levels up to 100% of the native material strength. The bonding tests were performed in normal joint compression and shear across the bedded plane in sub-size specimens. While not directly analogous to geologic materials, the layered PMMA specimens would allow for a controlled study of bedding and its influence on wave transmission and fracture evolution. Velocity anisotropy of the cubes was characterized as being between 2755 m/s for the bulk material velocity and 2735 m/s when measured perpendicular to several layers.

Multiple boreholes were formed into the cubes to assess inter-connectivity across a mock EGS reservoir configured for sources to be detonated simultaneously. Two bores were spaced 6 cm apart to provide a distance of approximately 8 borehole diameters for fracture growth. The boreholes were oriented perpendicular and parallel to the bedding planes for observing the relative effect these variables had on the fracture system.

In order to simulate geologic overburden, a hydraulic press was employed to apply a compressive stress (σ_1) to the cube faces. Tooling was fabricated to bring the samples to the correct elevation for shadowgraph imaging and to accommodate detonator wiring. The tooling also provided a backstop for miniaturized sealing elements at the top of the wellbore preventing the loss of source gas critical for driving fractures.

1.2. Experimental Diagnostics

High speed shadowgraph techniques were employed to view the response of the PMMA block. Schlieren and shadowgraph imaging are methods that capture a change of refractive index, or how light propagates through a transparent material [9]. These are useful diagnostics as the refractive index is proportional to the material density. Stress induced change in density is analogous to the high-speed shock traveling through the material. The images derived may be compared to computational models at various time steps. A setup of the schlieren imaging system consisting of a light source, collimating and focusing parabolic mirrors, a knife edge and a high-speed camera can be seen in the figure below. The area between the parabolic mirrors housed the PMMA blocks as shown in Figure 2. Imaging was prepared for the experiments with at 1 million frame per second (FPS) and either a 30 or 36 kFPS camera so that prompt events and later time fracture growth could be captured.

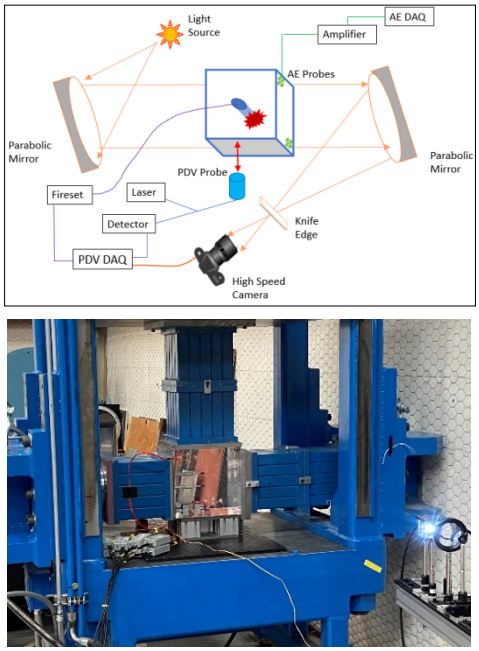

Fig. 2. Instrumentation Diagram (Top) and Physical Test (Bottom) showing: Target, Source, Shadowgraph, PDV and AE elements housed within a hydraulic press

Photon Doppler Velocimetry (PDV) has been used to measure the shock velocity, particle velocity, free and internal [10] surface velocities. In this study it is used to collect the particle velocity of a free exterior surface parallel to the cylindrical borehole loaded with the RP-80 source. This technique directs a laser pulse at a surface, which reflects and is collected and compared to a reference laser pulse. If the reflecting surface is moving at a velocity, the reflected light is frequency (Doppler) shifted from the reference laser pulse, which is the desired measurement [11]. The reference and reflected laser illumination are combined to produce an interference pattern, which is proportional to the surface velocity. This signal is converted into an electrical signal by fast photodetectors and recorded on a 12 GHz oscilloscope. Due to the transparent nature of the PMMA substrate the exterior surface had to be prepared with a reflective tape.

Acoustic emission sensing was integrated into outer surface of the cubes to allow for detection of fracture hypocenters. Transducers were utilized in arrays positioned on the same cube face on diagonal corners or on opposing sides on diagonal corners. The use of arrays having four relative arrival times allows for 3D analysis of a hypocenter location using a simplex error minimization function [12,13,14]. Application of the simplex method to AE instruments requires the use of a

uniform media with a constant wave speed, v [13]. For i_{th} sensor with an observed arrival time t_{oi} and a calculated arrival time t_{ci} is given by Eq. 1 as:

$$\gamma_i = t_{oi} - t_{ci} \quad (1)$$

This is the difference in a wave arrival time versus a calculated arrival time for an initial emission location (1) given by Eq. 2:

$$\gamma_i = \frac{\sqrt{(x_i - x_s) + (y_i - y_s) + (z_i - z_s)} - \sqrt{(x_1 - x_s) + (y_1 - y_s) + (z_1 - z_s)}}{v} \quad (2)$$

Where x_s, y_s and z_s are unknown coordinates of the source. For a 3D location at least three sensors are required for the solving source coordinates. This is performed on a step basis while residuals or error (γ) is minimized across all channels by the sum of squares [14]:

$$\chi^2 = \Sigma(\gamma_i)^2 \quad (3)$$

While other location algorithms exist, the simplex method requires only algebraic evaluation not derivative methods which makes it computationally effective. Additionally, it is very robust as it will not leave a low error location if a better (lower) one may be found [13].

Acoustic coupling of the sensor faces was accomplished using glucose syrup before applying a temporary adhesive bonding around individual sensor circumferences to prevent debonding from strong prompt shocks acting on the sensors rear surface. The Nano-30 sensors manufactured by the Mistras group sensors were connected to a Physical Acoustics Detection system sampling at 10 million samples per second (10Msps) and was triggered by first arrival waveforms amplified to 40 dB with the triggering threshold set to 45 dB.

In order to understand the complex phenomenon that explosives can induce, numerical simulations of the experiments have been performed using GEODYN/GEODYN-L hydrocodes developed at Lawrence Livermore National Laboratory. These tools are useful for observation of wave propagation and interaction as well as the effects of volumetric defects such as previously existing fractures [15]. GEODYN-L is a Lagrangian hydrocode, and despite the large deformations associated with energetic events it can avoid excessive mesh distortion by use of a dynamic adaptive remapping algorithm. It is also capable of allowing multiple materials in each element which will be critical for capturing interaction of gases with the PMMA within fracture interfaces [15].

2. EXPERIMENTATION AND RESULTS

The experiment series was performed at New Mexico Institute of Mining and Technology's Energetic Material Research and Test Center (EMRTC) in Socorro NM. The RP-80s were placed into the borehole of the PMMA cube before tamping with 40/70 mesh ceramic proppant. The proppant was primarily intended to reduce free volume within the cavity so that gasses could spend less energy compressing any air in the borehole. A feed through was provided for the firing signal to reach the detonator through a sealing bulkhead made from a small mandrel and a tapered rubber plug. Initiation of the EBW source resulted in fractures of the PMMA surrounding both borehole sources in all the cube specimens.

Figure 3 shows a series of images collected by the high-speed imaging system of an unstressed monoblock sample with two sources.

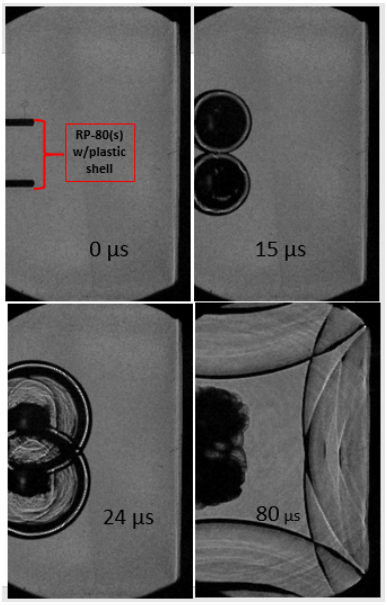

Fig. 3. Shadowgraphs of an unstressed dual detonation explosion process showing shock wave interactions and reflection from the cube surfaces as well as fracture growth.

Beginning at approximately 6µs after the trigger, the sources begin to create compression waves onto the PMMA. These primary waves begin interacting as source propagates this pressure radially as the detonation front progresses radially outward from the sources. At approximately 15µs the primary shocks continue to grow radially interacting through one another and continuing to grow (24µs). The subsequent closed volume explosive pressure caused in the cavity is less than the interface

conditions and decays thereafter as fractures form and the cavity grows, allowing for further transient pressure drop.

The emergence of coherent fractures first occurs around 40μs. In this sense, these fractures and cracks appear to be caused by the source and not reflections or interaction with target boundaries. At approximately 50μs the coherent fractures from each source begin to interact. The fractures first appear as slightly shaded regions with a darker leading edge as shown in Figure 4 at 60μs. This suggests a change in the refractory index at the fracture tip due to a highly localized increase in stress state.

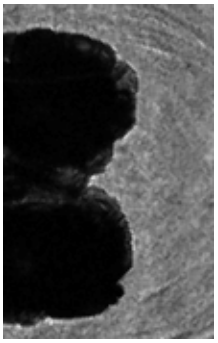

Fig. 4. Shadowgraph at 60μs w/ darkened bands

Previous experimental observations, lead investigators to believe the stress state build up and released periodically from later time source gas pressure, this is apparent in the fracture facets as shown in Figure 5 below imaged with the 30 kFPS system.

Fig. 5. Monoblock unstressed shadowgraph at 600μs

Later time artifacts of the fracture network can be observed by darkened regions caused by a substantial change in refractive index. In this case the darkened region may not be due to an increase in density driven by stress, but rather a combination of discontinuity (fracture) densities, orientations and fracture heights filled with hot product gasses rendering the stimulated volume opaque.

In the unstressed example above, acoustic emissions had not yet been employed, so observations of the fractures were only optical as PDV did not have enough probes in the array and low signal to noise ratio for observation of the weak elastic waves that are released by the fractures.

Adding stress to the experiment did not appear to significantly change the early high-speed images, but towards the 80 μs mark fractures appear less opaque in the areas behind the tip region.

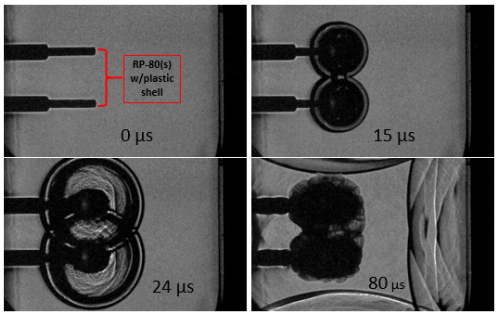

Fig. 6. Shadowgraphs of a stressed dual detonation explosion; σ_1 applied vertically in this image

Here the fractures still darken the image due to the difference in refractive index of the PMMA, however the fractures generated appear to be growing more perpendicular to the field of view (FOV) relative to the unstressed experiment (Figure 7 vs 5). From a high-speed imaging perspective, the 2 MPa applied stress appeared to limit the directionality of fracture growth.

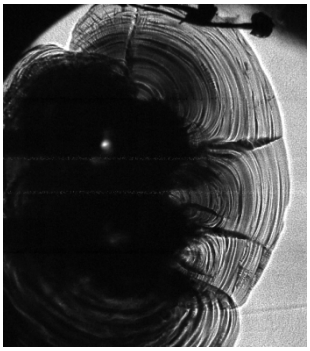

Fig. 7. Monoblock stressed shadowgraph at 610μs; σ_1 applied vertically in this image

Post-test examination of the stressed and unstressed monoblock samples yield differences in the way that the fracture networks form. The unstressed monoblock displayed cracks growing near the source randomly and

later time fractures growing in several directions away from the wellbore as seen in Figure 8. Several of these fractures are growing in and out of the field of view as well as vertically connecting the small boreholes and extending beyond them. On the right side of Figure 8, the stressed monoblock shows a more orderly fracture network that has formed vertically between the two small wellbores and beyond them where one fracture reached the outer surface of the cube. In the case of the stressed cube there are fewer fractures misaligned with the direction of σ_1(vertical).

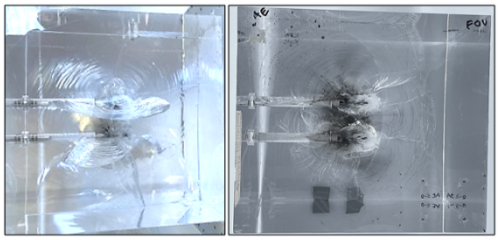

Fig. 8. Post-test monoblock cubes. Unstressed (Left); Stressed (Right); σ_1 applied vertically in this image

The difference in application of stress in the case of these two monoblocks had little influence in the nearfield (< 2 wellbores diameters) fracture networks but did result in visible changes to the intermediate and far field gas driven fractures.

Interrogating the AE sensors of the stressed sample provide significant insight to the creation of the fracture network. Unlike typical AE testing, the use of energetics generates strong prompt shock creating highly discontinuous volumes of damaged material. This can be best visualized with a time series scatter plot as shown in Figure 9 below.

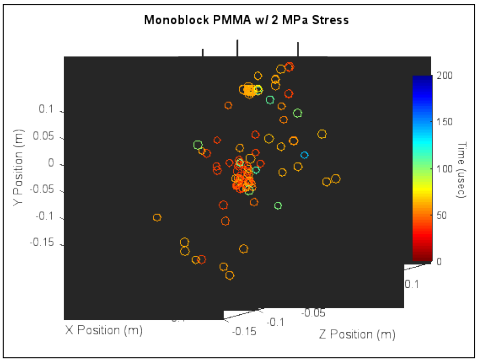

Fig. 9. AE of stressed monoblock. σ_1 applied in the Y-axis. FOV along X. Darker colors correlate to later arrivals (µs). Marker size indicates relative emission amplitude.

While prompt fractures become visible in the shadowgraph images at 40µs, AE diagnostics begin to detect collocated emissions in the same timescale when expected wave arrival (computationally modeled at 48 µs) is subtracted from the AE system time. AE in the near wellbore region the earliest events are co-located, with over 1000 waveforms appearing on the sensor array. Error minimization of the emission locations resulted in over 100 high quality co-located events with a high density in the volume between the two wellbores, suggesting a cluster of prompt damage.

Differentiating between the AE and shadowgraph modalities in the ZY plane allows for a direct comparison as shown in Figure 10. Overlaid onto the AE plot is a shadowgraph at 50µs.

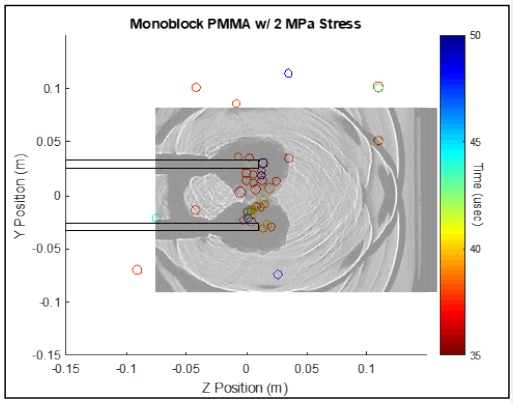

Fig. 10. Scaled shadowgraph at 50µs overlaid on AE of stressed monoblock. Boreholes represented by black rectangles.

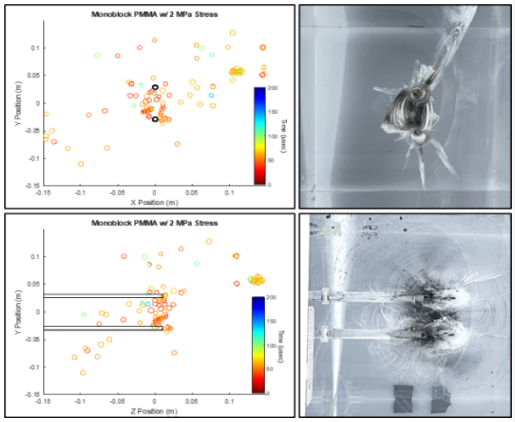

Fig. 11. AE of stressed monoblock (Left) and Photo (right) in the XY (Top) and ZY (Bottom) planes. Boreholes represented by black circles or rectangles.

There appears to be good correlation of the events both a in spatial and temporal sense for the prompt fractures seen in the shadowgraph as the AE system had detected 45 emissions up to this point. The AE data may also be compared to the post-test artifacts using the XY or ZY planes. In Figure 11 above the area of interest forms an elliptical fracture pattern between the two wellbores which is visible in XY plane emissions data and photographs in the same direction.

While the elliptical fracture network connecting the two sources is what is desired for an EGS system, other features such as the stray fracture that extends to the free face of the cube are less desirable. An important point in this work is that co-located emissions do not always correlate to a fracture. This can be seen by numerous AE events that would appear to be spurious as they go unwitnessed by images. Other inaccuracies exist such as fractures that are not observed by AE and may not meet the simplex location search threshold.

The use of AE in the presence of strong compression waves is a field under investigation. Implementation of the simplex algorithm for error minimization assumes the fundamental use of a wave having a single sound speed to all sensors in an array which could introduce significant error when transient stresses or attenuation is present.

Overestimation of microcrack activity is not unique to this study. Interaction of waves such as those seen in shadowgraph images could be correlated by the AE system as an event with a hypocenter as the resultant wave was emitted. However, missed microcrack emissions could be explained by weak elastic waves interacting with strong boundary reflections. The reflected wave is experimentally observed returning to the prompt fracture tip at approximately 80µs on the shadowgraphs. The shock reflected towards the fractures would likely consume wavelet energy from a fracture release which would result in significant damping and dissipation.

In another configuration, horizontal wellbores and vertical stress were used with a layered target. This experiment used the same configuration of instrumentation however the layers introduced complexity by creating internal boundaries for reflections and attenuation of wave transmissions. The layered configuration captured less than half of the emissions of the equivalent monoblock sample.

An unfortunate side effect of such competent bonding is the introduction of residual stresses into the layers by the flattening of naturally convex or concave plates in the joining operations. This can be seen in Figure 12 below with areas near joints having significant differences in their refractive indices.

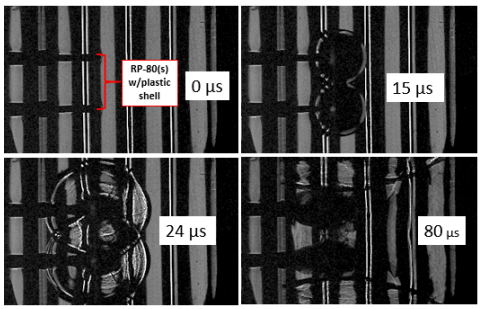

Fig. 12. AE of stressed monoblock (Left) and Photo (right) in the XY (Top) and ZY (Bottom) planes. Boreholes represented by black circles or rectangles.

An important point regarding the first arrival that triggered the AE data capture is that it is heavily dependent on the wave path to the sensor. In the case of layered targets, layer impedance plays a critical role in the directional velocity. Virgin layered PMMA cubes showed a marginal degree of velocity anisotropy which was valid for initial spatial-temporal correlation of emissions. However, for both cube types, induction of damage caused changes in velocity and possible differences in AE sensitivity across the array.

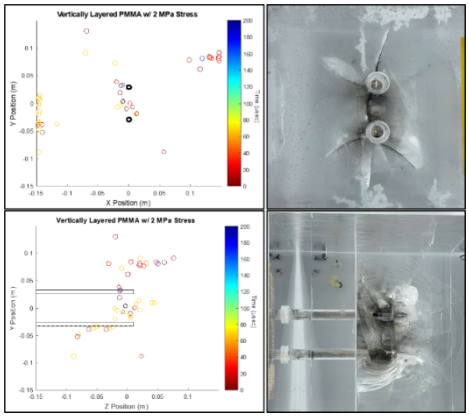

Fig. 13. AE of layered and stressed cube (Left) and Photo (right) in the XY (Top) and ZY (Bottom) planes. Boreholes represented by black circles or rectangles.

AE data may also be compared to the same post-test artifacts of the layered cube using the XY or ZY planes of the layered cube. In Figure 13 above, the area of interest forms a single fracture between the two wellbores which is visible from emissions data and photographs. Of note in this testing, a fracture formed in the second layer interface from the left of Figure 13 (visible in lower right frame). Clusters of emissions were detected where the wellbore and outer surface interfaced with the layer.

Assessment of the near source microcrack velocities was performed by rotating the images 90° and applying the streak technique where a column of pixels was inspected for the leading edge of the fracture fronts moving towards the inter-well volume desired for connectivity.

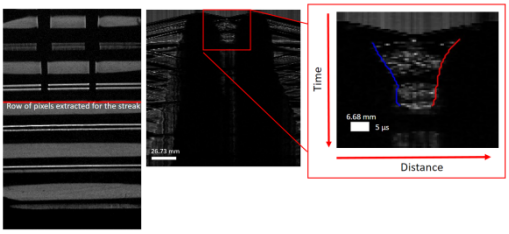

Fig. 13. Rotated image for streak w/ selected pixel row (Left), resulting streak image (Center) and the area of interest (Right) with polynomial fracture front fits (blue and red).

The pixel row location was chosen with an initial state with visual refractivity close to the unstressed state. The polynomial fit for the velocities shown in Figure 13 were 323 and 262 m/s: blue and red respectively. AE measurements may be used to filter candidate events to derive a front velocity by creating a sphere to consider possible secondary locations indicating feature growth.

The filtering for this technique involves creating a volumetric sphere around an early time event and looking for a second emission within the sphere occurring at a later time. An example for correlation to streak imaging is shown below in Figure 14.

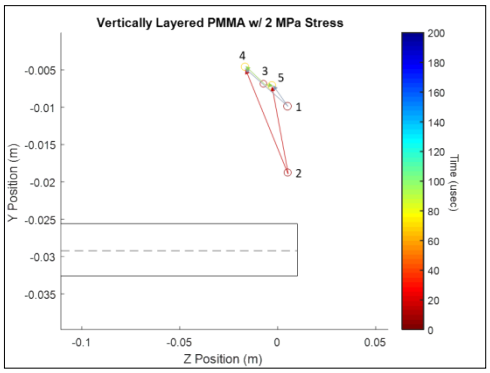

Fig. 14. AE of layered and stressed cube in the ZY plane. Isolated by emission location and time w/ 6 possible fracture paths. Lower bore represented by rectangle.

First points were chosen with a time less than 10µs, and a sphere with .035m radius. The resulting velocity calculations are presented below in Table 1.

Table 1. Experimental 3D and (2D) Fracture Velocities between emission points

	3D & (2D) Velocity (m/s)	
Points	P4	P5
P1	387 (359)	279(136)
P2	584 (418)	556(228)
P3	363(166)	435(74)

While the use of emissions data may not be entirely useful for detecting fracture velocity, it may be possible to improve this technique. An important point regarding the streak image velocity is that it is taken as a planar velocity in the ZY plane, and the AE data is taken as 3D. Both are shown for comparison strain rate dependent data from Kobayashi [16]. These data suggest that Mode 1 fractures in PMMA close to their origin can grow from 180 m/s for strain rates near 1 x 10^{-7} or as high as 380 m/s for strain rates near 48 1/s. The data taken by Kobayashi was presented as velocity versus distance from the fracture origin, in this work we would fall on the low end of distances considered. For this work (Figure 14 and Table 1), velocities of interest are calculated at distances of 8 to 25 mm between emissions. Unlike other research, the use of explosives generates a stress cage which fractures must contend with. The cage effect can cause any joint or aperture to slide, making AE difficult to deconvolute.

Calculation of relatively slow fracture speed, such as those in far field are not supported by other researcher's data and are most likely; non-correlated events or the result of fracture cycling which has been observed as growth-arrest-growth in the shadowgrams. Significant wave attenuation created by prompt damage between emission source and sensor is yet another likely cause of uncaptured events. Post experiment velocities were also examined by sonic testing as shown in Figure 15 below.

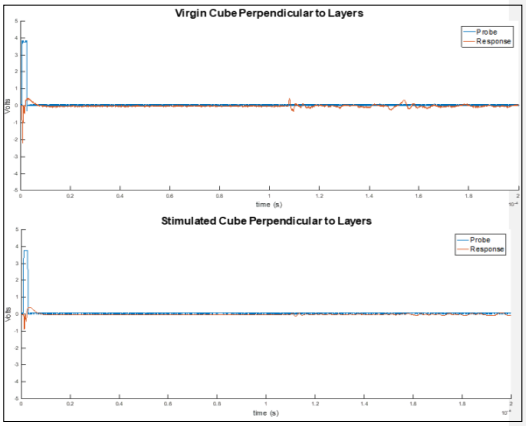

Fig. 15. Velocity profiles of virgin and stimulated cube.

Significant attenuation resulting from the delamination was observed when interrogating the layered cube in the direction perpendicular to the joint (along the Z axis). The aperture caused by the delamination effect is hypothesized to be a major cause of emission signal loss.

Computational efforts [17] running parallel to this experiment series are being informed on the growth of the shock induced damage or bulking. The simulations agree well with shadowgraph images for shock progression. In Figure 15 below the bulking front (dark green) can be seen at the inter-well volume at approximately 96 microseconds. This damage is not correlated to fracture, but a volume of material with increased permeability from shock pulverization.

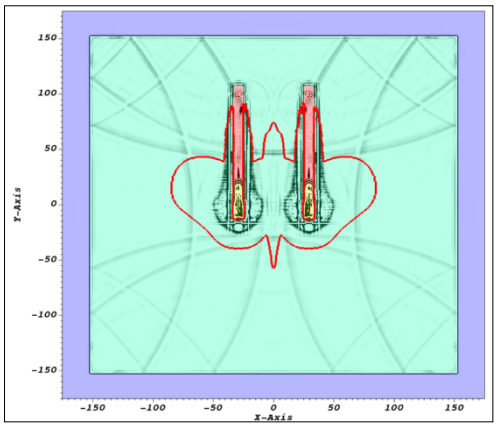

Fig. 15. Computational model at 96μs of a monoblock. Dark green represents damaged volumes of surrogate. Red is elastic boundary.

Model improvements are currently underway to evaluate computational methods and efficiencies of including fracture behavior based on these data. This involves the coupling of a fluid solver to account for the source gas effect the GEODYN hydrocode.

3. KEY POINTS AND FUTURE WORK

Observations from this study of scaled energetic stimulation may be distilled down into several interesting phenomenon.

First that the application of stress for these sources combined with the PMMA simulated geology may result in directional order of fractures resulting in a shared fracture network between two wellbores.

Secondly, AE has demonstrated the ability to detect damage activity in the inter-well volume of this system. While not statistically significant, fracture velocities have been correlated to the regimes of other researchers using AE sensing in the inter-well volumes of interest.

Lastly, artifacts such as false emissions and missed fractures are inherent to the sensing system and algorithms used. The performance of AE while using energetic sources to induce loading is not well studied. The experiment configurations herein may be near the limits of event detection due a combination of strong source waves, their interactions, and small heavily damaged surrogate volumes.

Lastly, this test series has provided a foundation for the transition to opaque geologic materials in a follow-on study. This will present a new set of challenges and the authors are developing tools to correlate emission sensing to computer tomographic imaging. Further evaluation of the energetic stimulation concept and improving fidelity of the computational model be direct results of the next series.

4. ACKNOWLEDGEMENTS

The authors wish to thank the Geothermal Technology Office of the U.S Department of Energy for sponsoring this work. They would also like to thank Charles Choens for his advisement on the use and theory of AE, as well as Mathew Ingraham for his acoustic measurement expertise and guidance on AE practices.

Sandia National Laboratories is a multi-mission laboratory managed and operated by National Technology and Engineering Solutions of Sandia, LLC., a wholly owned subsidiary of Honeywell International, Inc., for the U.S. Department of Energy's National Nuclear Security Administration under contract DE-NA-0003525.

The work by Lawrence Livermore National Laboratory was done under Contract DE-AC52-07NA27344.

Funding for this work at New Mexico Institute of Mining and Technology (New Mexico Tech) is provided by Sandia National Laboratories via PO 2179527.

REFERENCES

1. EPA. 2016, Hydraulic Fracturing for Oil and Gas: Impacts from the Hydraulic Fracturing Water Cycle
2. Grubelich, M., 2015. An Overview of High Energy Stimulation Techniques for Geothermal Applications. *OSTI. 1248651, SAND2015-2614C*
3. Mumma, D., McCullough, F., Schmidt, E.W., Pye, D.S., Allen, C.W., Pyle, D., and R.J. Hanold. 2015. GEOFRAC- An Explosives Stimulation Technique for a Geothermal Well of High Energy. *Geothermal Resource Council Meeting, 11-14 October 1982. LA-UR-82-2020*

4. Cuderman, J.F., Chu, T.Y., Jung, R.D, and R.D. Jacobson. 1986. High Energy Gas Fracture Experiments in Fluid-Filled Boreholes- Potential Geothermal Application, Sandia National Laboratories, SAND85-2809

5. Robey, R.E., Pope, J.S., Vorobiev, O.Y., Torres, S.M., Hargather, M.J., Kimberley, J., Mann, D., 2021. Lab Scale Study of Energetic Gas Stimulation in Engineered Materials. 55th US Rock Mechanics/Geomechanics Symposium. ARMA 21-1219

6. Bastea S., Fried L.E., Glaesman K.R., Howard W.M., Kuo I.F., Nimmakala S., Souers P.C., Taller D., and P.A. Vitello. 2019. CHEETAH 9.0 User's Manual, Energetic Materials Center, Lawrence Livermore National Laboratory, LLNL-SM-769619

7. Rae P.J., A Review of the Mechanism by which EBW Detonators Function, Los Alamos National Laboratory, LA-UR-18-31181, 2018

8. Cooper, P.W. 1994. *Explosives Engineering*. 1st ed. Hoboken NJ: John Wiley and Sons.

9. Settles, G.S., 2001. *Schlieren and Shadowgraph Techniques: Visualizing Phenomena in Transparent Media.* Berlin: Springer.

10. Jordan J.L., Casem D., and Zellner M., 2019. Shock Response of Polymethylmethacrylate. J. Dynamic Behavior of Mater. 3: 372–78

11. Ward, S., Braithwaite, C., and A. Jardine. 2017. The Effects of Nanostructure upon the Dynamic Ductile Fracture of High Purity Copper, Procedia Engineering, DYMAT 23rd Technical Meeting- International Conference on Dynamic Fracture of Ductile Materials 197: 23-32

12. Nelder, J.A., and R. Mead. 1965. A Simplex Method for Function Minimization. The Computer Journal. 4: 308-313

13. Ge, M. 2003 Analysis of source location algorithms part II: iterative methods[J]. Journal of Acoustic Emission 21(1), 29–51

14. Mistras Group. 2014. Express-8 AE System User's Manual.

15. Vorobiev, O.Y. 2012. Simple Common Plane contact algorithm. *Int. J. Num Meth in Engineering.* 90: 243–268.

16. A. Kobayashi, N. Ohtani, T. Sato. 1974. Phenomenological aspects of viscoelastic crack propagation. J. Appl. Poly. Sci., 18 , pp. 1625-1638

17. Vorobiev,O.Y., Robey, R.E., Pope, J., Torres, S.M., Hargather, M.J., 2022. Analysis and Modeling of Explosive Fracturing Process in a Transparent Surrogate of Jointed Rock. 56th US Rock Mechanics/Geomechanics Symposium. ARMA 22-90.